Environ Sci Pollut Res (2013) 20:4009–4017
DOI 10.1007/s11356-012-1364-4

RESEARCH ARTICLE

A study on the self-assembly behavior of dark materials from molasses

Ken-ichi Hatano · Isamu Komatsu · Naokazu Aoyagi · Kazuki Takahashi · Kenji Kubota

Received: 10 September 2012 / Accepted: 22 November 2012 / Published online: 5 December 2012

Abstract We have previously demonstrated that dark materials (DM) in acidified molasses are effectively adsorbed to Amberlite XAD7HP resin and are eluted from the resin with 0.1 M sodium hydroxide. In this paper, we have characterized the self-assembly behavior of molasses DM by using dynamic and static light scattering in combination with isoelectric focusing and infrared absorption spectroscopy in order to better understand the resin adsorption mechanism. One of DM derivatives, X-G2, contained carboxyl and hydroxyl groups and had a weight-average molar mass of 9.39×10^3 to 4.42×10^4 at pH 2.1–11.5. The aggregates retained their spherical shape over the full pH range and the large gyration radius (66.4–80.0 nm) indicated that the inner structure was loosely packed. Furthermore, X-G2 had an isoelectric point of 1.8, and its density increased sharply at pH 5.9 and then approached a nearly constant value under alkaline conditions. In summary, the self-assembly processes of DM are controlled by intermolecular hydrogen-bonding and hydrophobic interactions. The aggregates adsorb to the resin through hydrophobic interactions and are eluted when excess carboxylate anions are generated.

Keywords Dark materials · Infrared spectroscopy · Isoelectric focusing · Light scattering · Self-assembly behavior · Sugarcane molasses

Responsible editor: Philippe Garrigues

K.-i. Hatano (✉) · I. Komatsu · N. Aoyagi · K. Takahashi · K. Kubota
Department of Chemistry and Chemical Biology, Graduate School of Engineering, Gunma University, 1-5-1 Tenjin-cho, Kiryu, Gunma 376-8515, Japan
e-mail: hatano@gunma-u.ac.jp

Introduction

The high worldwide demand for energy, the uncertainty of petroleum resources and concern about global warming has led to the development of alternative environmentally friendly liquid fuels. Ethanol is regarded as one of the good candidates, since it reduces dependence on fossil fuel reserves and it is also cleaner burning and thus better for air quality. Biomass ethanol can be produced from a wide range of feedstock, including sugar-based, starch-based, and cellulosic materials. Sugar-based feedstock contains readily available fermentable sugars, and recent research has demonstrated that sugarcane and sugar beet molasses, which are by-products of sugar manufacturing, show high ethanol productivity and are renewable substrates. However, there are serious environmental problems with sugar manufacturing and molasses fermentation which are mainly related to the production of a brown effluent, known as vinasse or spentwash. The amount of vinasse can be up to 10-fold greater than that of the ethanol produced. The colorants are produced during sugar manufacturing by non-enzymatic browning reactions, such as the Maillard reaction (melanoidins), alkaline degradation reactions (hexose alkaline degradation products; HADP), and sugar degradation (caramels; Coca et al. 2004).

Vinasse is characterized by extremely high chemical oxygen demand (COD) and biochemical oxygen demand (BOD), low pH, a strong odor, and a dark-brown color. It is usually subjected to conventional anaerobic and aerobic wastewater treatments, such as methane fermentation and activated sludge treatment, which easily remove organic matter and reduce the COD and BOD. However, these treatments do not decompose or decolorize dark materials (DM) in vinasse because of its high COD (90,000 mg/L) and BOD

(40,000 mg/L; Chuang and Lai, 1978), and the presence of other toxic components (FitzGibbon et al. 1995; Chandra and Pandey 2001). When DM are discharged into surface water, they reduce sunlight penetration in rivers, lakes, and lagoons, which in turn decreases both photosynthetic activity and dissolved oxygen, thereby severely affecting aquatic life. The disposal of DM on land is equally hazardous; they inhibit seed germination and deplete vegetation by reducing the soil alkalinity and manganese availability (Agarwal and Pandey 1994; Kannabiran and Pragasam 1993). Thus, vinasse must be pretreated before it can be safely disposed of in the environment. DM from sugarcane molasses possess components in the same molecular mass range (<22,000), which consist of melanoidins, HADP, and caramels (Mersad et al. 2003).

In the past, vinasse has been degraded and decolorized by activated carbon adsorption or biological decolorization using fungi and by chemical methods (Chandra and Singh 1999) or by flocculation and physicochemical treatment, such as ozonation (Kim et al. 1985). However, these methods are not economically feasible on a large scale because of their cost. Recently, we demonstrated that the fractions of sugar and DM could be effectively separated from sugarcane or sugar beet molasses by dilution, acidification and adsorbent-column chromatography (Hatano et al. 2008). The color of the resulting wastewater was reduced by 87 % through our approach, compared with conventional molasses fermentation, and the recovery of DM was 53–65 g/L sugarcane molasses for pH 1–4 and 3- to 10-fold dilutions. Furthermore, the decolorized molasses retrieved from the adsorbent column showed excellent fermentation efficiency almost equal to the original molasses (Hatano et al. 2009). However, the self-assembly behavior of DM has not been examined.

In this paper, we have determined the self-assembly behavior of DM and have proposed a mechanism for the adsorption of DM onto Amberlite XAD7HP resin, which mainly depends on pH. The structures of DM were characterized by visible and infrared (IR) absorption spectroscopy, isoelectric focusing, and light scattering (LS) analysis.

Materials and methods

Materials and adsorption rate

Two types of sugarcane molasses, denoted as Meiji and Fuji molasses, were kindly donated by Dai-Nippon Meiji Sugar Co., Ltd. and Fuji Nihon Seito Corporation, Japan, respectively. Sugar beet molasses was provided by Hokkaido Sugar Co., Ltd., Japan. Crude sugar produced from sugarcane grown in Thailand was provided by Fuji Nihon Seito Corporation. The Amberlite XAD7HP and IR120B resins were purchased from Organo Corporation (Tokyo, Japan). Commercial bovine hemoglobin was purchased from Tokyo Chemical Industry Co., Ltd. (Tokyo, Japan). For DM derivatives, the X samples were separated from the acidified molasses of Meiji, Fuji or sugar beet by using an XAD7HP column. The X-Meiji sample was separated on a Sephadex G-50 column into early and late peaks, which corresponded to the X-G1 and X-G2 samples (Hatano et al. 2008). The 10 mg/mL X-Meiji solution was adjusted to pH 1.0 and was centrifuged at 12,000×*g* at room temperature for 10 min. Then, the X_{pre} precipitate and X_{sup} supernatant samples were recovered. All other reagents used were of the highest grade commercially available.

In order to examine the adsorption rate of the DM to the resin, 20 mg/mL X-G2 solution (1 mL) was applied to an XAD7HP column (1.5×7 cm) at room temperature. The resin in the chromatographic tube was rinsed with ultrapure water (30 mL), and then the X-G2 sample adsorbed was eluted from the resin with 0.1 M sodium hydroxide (NaOH; 10 mL). The adsorption rate of X-G2 was calculated using the following equation:

$$\text{Adsorption rate}(\%) = 100(A_{total} - A_{unad})/A_{total} \quad (1)$$

where A_{unad} is the summation of product of the fraction volume (5.5 mL) and the absorbances at 420 nm (mL×A_{420}) in the flow-through peak from the column, and A_{total} is the product of the sample amount loaded on the column (1 mL) and the A_{420} value (39.5). In the adsorption experiment, 10 mM glycine–HCl, acetate, sodium phosphate, and Tris–HCl buffers were used as elution solutions at pH 2.1, 4.1, 5.9, and 7.3–11.5, respectively.

Spectroscopic analyses

The sample (3 mg) and potassium bromide (200 mg) were mixed and pressed into disks (2 cm in diameter) in a pressing machine at a constant pressure of 200–400 kg/cm^2 under vacuum. For each IR spectrum, 64 scans were taken at a resolution of 8 cm^{-1}. Fourier transform infrared (FT-IR) spectra were recorded at 20 °C on a Nicolet Magna560 Continuμm FT-IR spectrophotometer (Thermo Fisher Scientific, Madison, WI) at wavenumbers of 400–4,000 cm^{-1}. The measurement chamber was purged with nitrogen gas for 20 min to avoid carbon dioxide and moisture interference.

The E_4/E_6 ratio of DM derivatives was determined by measuring the absorbances at 465 and 665 nm on a UV-1800 spectrophotometer (Shimadzu, Kyoto, Japan). For measurement, the concentration and pH of all the derivatives were 1.0 mg/mL and pH 7.5, respectively.

Cation exchange capacity

The cation exchange capacity (CEC) was determined by a conventional acid–base titration experiment. An ion-

exchange column (1.5×11.3 cm) was packed with Amberlite IR120B resin, and the resin was protonated with 2 M HCl (500 mL). The 1.0 mg/mL X-Meiji or X-Fuji sample (100 mL) was applied to the column, and the protonated sample was collected as a flow-through peak and was lyophilized to powder. The protonated sample (1.0 mg) was dissolved in ultrapure water (10 mL) in a beaker. The solution was titrated with 0.1 M NaOH, and the pH value was recorded at 20 μL increments. The inflection point of the acid–base titration curve was analyzed using the program PKA-I (Tanokura et al. 1976), and the most probable value and standard deviation were obtained for the macroscopic pK_a value.

Isoelectric focusing

Analytical isoelectric focusing of DM derivatives was performed by paper electrophoresis at room temperature. A 10 mg/mL sample solution was prepared, and the pH was roughly adjusted to values between 1 and 13 by using HCl or NaOH. Each sample solution (5 μL) and the corresponding buffer (5 μL) were mixed and incubated for 1 h. The buffers were McIlvaine wide-range buffer (pH 1.0–9.0) and 0.3 M sodium bicarbonate buffer (pH 8.0–13.0). The sample solution (5 μL) was applied to a filter paper (100×10 mm), and the paper was placed on a glass plate and dipped into the buffer. Both ends of the paper were clamped with bulldog clips connected to a power supply. Electrophoresis was carried out for 20 min at 150 V, and the migration length of the sample spot was visually measured after the filter paper was dried. The control experiment using bovine hemoglobin was performed in the same way.

Dynamic and static light scattering

The sample concentration (c) was adjusted to 0.5, 1.0, 1.5, or 2.0 mg/mL by using ultrapure water, 0.1 M sodium chloride (NaCl), 0.1 M sucrose, 1 mM ethylenediaminetetraacetic acid (EDTA), or 1 mM copper sulfate ($CuSO_4$), and the sample solutions were adjusted to the appropriate pH. The sample was optically purified in a clean dustproof box by filtration through a 0.45-μm nylon membrane filter (PALL, Port Washington, NY). An ALV-5000/E multiple-τ digital correlator was employed for the correlation function measurements in homodyne mode, and the scattered light intensity measurements were carried out simultaneously. A vertically polarized He–Ne laser with a wavelength (λ_0) of 632.8 nm was used as the incident beam. The vertically polarized scattered light was detected by a photomultiplier tube using the photon-counting method. Benzene was used as a standard for calibrating the scattering photometer (Pike et al. 1975). A cylindrical cell with an outer diameter of 10 mm was placed in a thermostat-controlled silicon oil bath at 25 °C with a constancy of 0.01 °C. The temperature was monitored by a calibrated platinum resistor. In the static LS measurements, the scattered light intensities at scattering angles of 30–135° were measured. The correlation functions were measured for 30–60° in the dynamic LS measurements.

Refractive index increments and data analysis

The specific refractive index increments ($\partial n/\partial c$) of the sample solution were measured for concentrations of 0.5, 1.0, 1.5, or 2.0 mg/mL at a wavelength of 632.8 nm using a DRM-21 double-beam differential refractometer (Otsuka Electronics Co. Ltd., Osaka, Japan). The temperature was set to 25 °C and controlled with a constancy of 0.1 °C. Zimm plots were employed to obtain the weight-average molar mass (M_w), the z average radius of gyration (R_G) and the second virial coefficient (A_2), which is expressed as follows:

$$Kc/\Delta R_\theta = \left(1 + < R_G^2 > q^2/3 + 2M_w A_2 c\right)/M_w \quad (2)$$

where c is the sample mass concentration (mg/mL), θ is the scattering angle and ΔR_θ is the excess Rayleigh ratio. The scattering vector is defined as $q=(4\pi n_0/\lambda_0)\sin(\theta/2)$, and the optical constant is defined as $K=4\pi^2 n_0^2(\partial n/\partial c)^2/N_A\lambda_0^4$, where n_0 is the refractive index of the medium and N_A is Avogadro's number. The autocorrelation functions of scattered light intensity ($G_2(\tau)$) were analyzed by the CONTIN method (Provencher 1982). $G_2(\tau)$ has the following form related to the normalized electric field correlation function $g_1(\tau)$:

$$G_2(\tau) = C\left[1 + \beta|g_1(\tau)|^2\right] \quad (3)$$

where C is the baseline and β is a machine constant relating to the coherence of detection. Generally, $g_1(\tau)$ is expressed by the distribution function ($G(\Gamma)$) of the decay rate and is expanded by the cumulant expansion:

$$g_1(\tau) = \int G(\Gamma)\exp(-\Gamma\tau)d\,\Gamma$$

$$\Gamma_{ave} = \int G(\Gamma)\Gamma\, d\,\Gamma \quad (4)$$

The z average translational diffusion coefficients (D_0) were estimated from the dynamic Zimm plots of Γ_{ave}/q^2 ($q\rightarrow 0$) versus c. The z average hydrodynamic radii (R_H) were calculated with the Einstein–Stokes equation, $R_H = k_B T/(6\pi\eta_0 D_0)$, where k_B is the Boltzmann constant and η_0 is the solvent viscosity.

Results and discussion

FT-IR measurements

The FT-IR spectra of DM derivatives were similar; in particular, the IR bands at 3,400, 2,950, 1,600, 1,400, 1,080, and 680 cm^{-1} were observed in all the spectra (Fig. 1). The strong broad band at 3,400 cm^{-1} was assigned to the hydrogen-bonding O–H stretching vibration (3,550–3,200 cm^{-1}), the band at 1,600 cm^{-1} was assigned to the carboxylate C=O or C–O stretching vibration (1,650–1,550 cm^{-1}), the band at 1,400 cm^{-1} was assigned to the carboxylate O–H stretching mode (1,420–1,330 cm^{-1}) and the band at 1,080 cm^{-1} was assigned to the alcohol C–OH or ester C–OC stretching mode (1,260–1,000 cm^{-1}). Moreover, the weak bands at 2,950, 1,250, and 680 cm^{-1} corresponded to the stretching vibration of aliphatic C–H (3,000–2,840 cm^{-1}) and phenol C–O (1,260–1,180 cm^{-1}) and the bending vibration of aromatic C–H (710–675 cm^{-1}), respectively. However, the IR bands at 3,400 and 1,600 cm^{-1} could, respectively, be assigned to the N–H stretching vibration (3,500–3,300 cm^{-1}) and the N–H bending mode (1,640–1,550 cm^{-1}), since the nitrogen content of X-Meiji was reported as 2 % (Hatano et al. 2008).

Thus, the DM derivatives contained carboxyl groups, hydrogen-bonding hydroxyl groups, aliphatic chains, and aromatic rings. However, the spectrum of X-G2 was a little different from that of X-G1; for example, the bands at 3,550–3,200, 1,650–1,550, and 1,250 cm^{-1} (Fig. 1). In a previous study, the molecule size of X-G2 was estimated to be smaller than that of X-G1, since the X-G2 fraction was eluted after the X-G1 fraction during gel filtration chromatography (Hatano et al. 2008). Probably, the carboxyl groups of X-G2 are more involved in hydrogen bonding than those of X-G1, and the molecular size of X-G2 may have decreased because of the overcrowded intermolecular hydrogen-bonding network among the carboxyl groups.

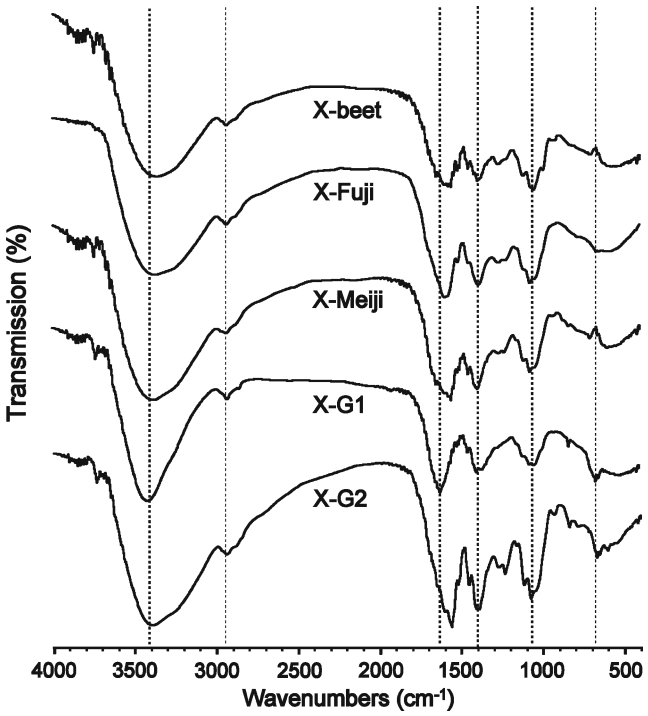

Fig. 1 FT-IR spectra of various DM derivatives. X-beet, X-Fuji, and X-Meiji were purified from sugar beet molasses, Meiji molasses, and Fuji molasses, respectively. The X-G1 and X-G2 samples were separated from X-Meiji by using gel-filtration chromatography. *Dotted lines* indicate common and important bands among DM derivatives

Isoelectric focusing, acid precipitation, cation exchange capacity and E_4/E_6 ratio

We measured the electrophoretic mobility of the X-G1 and X-G2 samples at each pH value (data not shown). As determined by the least-squares method, the isoelectric points (p*I*) of the X-G1, X-G2, X_{pre}, and X_{sup} samples were only 1.9, 1.8, 1.8, and 2.0, respectively. From the analysis of the acid–base titration, the CEC values of the X-Meiji and X-Fuji samples were estimated as 219±14 and 186±9 $cmol^{+}/kg$, respectively. For example, the CEC values for distillery waste co-composting with animal manure have been reported as 77–160 $cmol^{+}/kg$ (Bustamante et al. 2008). This suggests that all the DM derivatives are rich in acidic functional groups, such as carboxyl groups, which is consistent with the FT-IR results (Fig. 1). For comparison, the 10 mg/mL X-G1 aqueous solution was partially precipitated by adjusting the pH to 1.0, which indicates that the physical properties of the X-G1 sample may be similar to that of the X_{pre} sample. In contrast, no precipitation was observed for the 10 mg/mL X-G2 solution at pH 1.0.

The UV/Vis absorption spectra for all the DM derivatives showed no specific features, although absorbance steadily increased as the wavelength decreased; the E_4/E_6 ratio and the absorbances at 465 and 665 nm are listed in Table 1. The E_4/E_6 ratio has been used for the qualitative evaluation of humic substances, and the ratios reported for humic acid and fulvic acid are 3–5 and 6–8.5, respectively (Kononova and Aksenva 1963). We observed two main groups of E_4/E_6 ratios (Table 1), the X-G1 and X_{pre} samples had ratios of 7.0–7.3, and the X-G2 and X_{sup} samples had ratios of 11.0–14.1. The ratios for the X-crude sugar, X-Meiji, and X-Fuji samples lay between those of the two main groups, although the ratio for X-beet molasses was similar to those for X-G2 and X_{sup}. This would arise from the number of the condensation cycles in sugar production. In Japanese sugar factories, the number of cycles is always six for sugarcane syrup and is three for beet syrup. Therefore, the X-beet sample should contain simpler compounds and be a paler color than the X-Meiji and X-Fuji samples, because DM are formed mainly by the Maillard reaction during the sugar condensation

Table 1 E_4/E_6 ratios of DM from molasses-related resources

Sample name	A_{465}	A_{665}	E_4/E_6 ratio
X, crude sugar (X-crude)	0.960	0.113	8.50
X, sugar beet molasses (X-beet)	0.980	0.074	13.24
X, Fuji molasses (X-Fuji)	1.420	0.177	8.02
X, Meiji molasses (X-Meiji)	1.407	0.147	9.57
X-G1 from X-Meiji	0.819	0.118	6.94
X-G2 from X-Meiji	0.774	0.055	14.07
X-Meiji precipitate at pH 1	2.788	0.381	7.32
X-Meiji supernatant at pH 1	1.044	0.095	10.99

process. It may also arise from differences in the compounds present in the raw sugar beet and sugarcane juices, rather than the processing.

Molar mass and chain dimensions of DM and pH dependence

Figure 2 shows the angular (θ) and the concentration (c) dependence of Kc/R_θ (Zimm plot) for the X-G2 aqueous solution at pH 2.1, 5.9, and 10.2. The value of M_w was estimated by extrapolating c and θ to zero, and R_G and A_2 were calculated from the slope of the angular and concentration dependence of the Zimm plot, respectively. These numerical values are listed in Table 2, together with the data on R_G / R_H, density and adsorption rate. The value of R_G for X-G2 at pH 2.1–11.5 was much higher than that of myoglobin (1.8–3.0 nm), which possesses an apparent molecular weight of 17,800. Furthermore, the value of M_w for X-G2 increased from 9,390 to 44,200 g/mol as the pH increased, which indicates that the particles in X-G2 consisted of relatively small heterogeneous molecules and were self-assembled by hydrogen bonding or other weak forces (Hatano et al. 2008). The X-G2 particles had a low-density spongy structure, unlike globular proteins. The value of A_2 was near zero or positive for pH values of 5.9–11.5, while it was negative at pH 2.1 and 4.1 (Fig. 2, Table 2). When the A_2 value is positive, the aqueous solvent is a thermodynamically favorable for X-G2, and it is a poor solvent when it is negative. Therefore, the X-G2 particles were probably adsorbed to the XAD7HP resin because their surfaces were hydrophobic at pH 2–4, which is consistent with the result of the isoelectric focusing. The ratio of the radius gyration to the hydrodynamic radius (R_G/R_H) relates to the segment distribution and solvent permeability and reflects the chain stiffness (Burchard et al. 1980). The magnitude of R_G/R_H for spheres, vesicles, random coils, and rod-like structures is reported to be 0.78, 1.00, 1.78, and ≥2, respectively. Therefore, the small range of R_{Gz}/R_{Hz} (0.75–0.79) in the present study suggests that the X-G2 particles were spherical assemblies (Table 2).

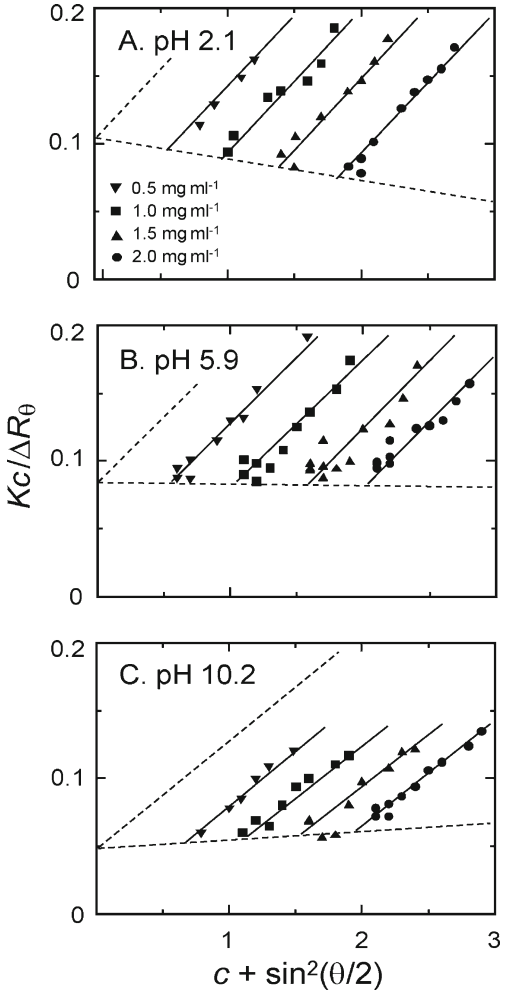

Fig. 2 Zimm plot of the X-G2 sample in water at **a** pH 2.1, **b** 5.9, and **c** 10.2, where the concentration changes from approximately 0.5 to 2.0 mg/mL. The *solid lines* are drawn to visualize the data points. The *broken lines* are indicative of extrapolating the concentration and angle to zero, respectively

Particle property of DM under various circumstances

The LS experiments for X-G2 were performed in the presence of the following additives: NaCl, EDTA, $CuSO_4$ and sucrose under the conditions as described in the previous section, except for the pH values (data not shown). In this section, we investigate the main force that controls the self-assembly behavior of DM. In the presence of 0.1 M NaCl, the M_w value of X-G2 at pH 4.1 (22,300) was 1.6-fold larger than that of the control experiment (14,200), and the other molecular parameters were similar to those of the control experiment (Tables 2 and 3). If the X-G2 aggregates flocculated through ionic bonding, the addition of salts should destabilize, should fragment the aggregates into small particles and should reduce the value of M_w. This suggests that the X-G2 particles are probably formed by

Table 2 Molecular parameters of X-G2 on the basis of static and dynamic light scattering data

pH	2.1	4.1	5.9	7.3	8.6	10.2	11.5
A_2	<0	<0	≒0	≒0	≒0	>0	≒0
M_w (g/mol)	9,390	14,200	37,000	41,800	43,900	44,200	22,200
R_G (nm)	68.3	69.0	70.6	73.1	75.0	80.0	66.4
R_H (nm)	91.0	89.0	91.2	93.2	97.5	102.1	85.2
R_G/R_H	0.75	0.78	0.77	0.79	0.77	0.78	0.78
Density[a] ($\times 10^{-5}$ g/cm^3)	1.17	1.71	4.17	4.25	4.12	3.42	3.01
Adsorption rate (%)	79	72	43	21	13	10	6

[a] The volume was calculated using M_w, R_G, and Avogadro's number

hydrogen bonding and the other weak forces. It is reasonable to assume that the addition of NaCl should neutralize the net negative charge of X-G2 and should strengthen the hydrophobic interaction, which is consistent with the result of the pH dependence (Table 2). Particle formation would be difficult through ionic binding, since the p*I* value is exceptionally low, which indicates that the number of positive charges was very small in comparison with the number of negative charges.

We have observed that DM can weakly chelate several metal ions (unpublished data); therefore, the X-G2 aggregates could be formed by the carboxyl or phenolic groups chelating metal ions. However, the M_w value in the presence of EDTA obtained from the LS experiments was 2-fold larger than that without EDTA (Tables 2 and 3), indicating that the aggregability and the M_w value were increased by the addition of NaCl and EDTA. However, the M_w value in 1 mM $CuSO_4$ (37,700) was 10 % lower than that of the control experiment at pH 7.3 (41,800; Tables 2 and 3). Interestingly, the adsorption rate of X-G2 in the presence of copper ions was more than 90 %, whereas the adsorption rate of the control experiment at pH 7.3 was 21 % (Tables 2 and 3). The positive charge of copper ions should promote aggregation and chelation and should neutralize the negative charge of the X-G2 carboxyl group. This should keep the molecular surface hydrophobic and adsorptive. The adsorption rate in the presence of 0.1 M NaCl at pH 7.4 (46 %) was much lower than the rate for 1 mM $CuSO_4$ (92 %; Tables 2 and 3). This indicates that X-G2 may chelate sodium cations less readily than copper cations. All four carboxyl groups of EDTA appear to dissociate completely at pH 4.1, because their pK_a values are 0–2.7 (Harris 2007). Therefore, the carboxyl groups of X-G2 could not dissociate easily due to mutual electrostatic repulsion, which increases the hydrophobicity of the molecular surface, thus increases the adsorption rate to the XAD7HP resin. The A_2 value in the presence of EDTA or $CuSO_4$ was negative, and the aqueous solutions were thermodynamically poor solvents for X-G2.

Three-fold dilutions of Meiji molasses were used in the decolorizing system, and the sugar concentration was 0.88 M (Hatano et al. 2009). In this LS experiment, the behavior of X-G2 in the presence of 0.1 M sucrose was examined, since sucrose is the major component of sugarcane molasses. The M_w value in the presence of sucrose was 1.5-fold larger than that in the absence of sucrose, although there was only a small difference in the values of R_G and R_H

Table 3 Molecular parameters of X-G2 under several solvents on the basis of static and dynamic light scattering data

Solute	0.1 M NaCl		0.1 M NaCl[b]	0.1 M sucrose	1 mM EDTA, 1 mM $CuSO_4$
pH	4.1	7.4[b]	4.1	4.1	7.4
A_2	<0	<0	>0	<0	<0
M_w (g/mol)	22,300	28,900	20,800	29,400	37,700
R_G (nm)	68.7	73.3	73.6	77.8	78.6
R_H (nm)	88.6	94.8	97.8	103.8	100.2
R_G/R_H	0.78	0.77	0.75	0.75	0.79
Density[a] ($\times 10^{-5}$ g/cm^3)	2.72	2.91	2.08	2.47	3.07
Adsorption rate (%)	82	46	71	93	92

[a] The volume was calculated using M_w, R_G, and Avogadro's number

[b] The absorption rate to XAD-7HP showed 73 % in 1.0 M NaCl and pH 7.4

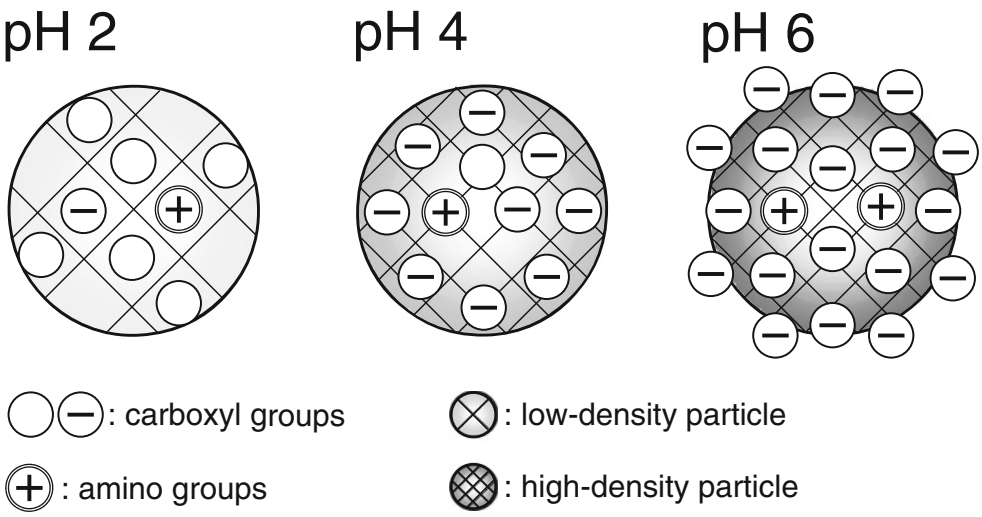

Fig. 3 Inside-charge and outside-charge distributions of the X-G2 particles at various pH values

(Table 3). The value of A_2 was positive in the presence of 0.1 M sucrose, although the adsorption rate was 71 % (Table 3). Accordingly, a negative value of A_2 is not required for X-G2 to adsorb to the XAD7HP resin. In addition, the surface of X-G2 would be covered with sugars and would be a thermodynamically good solute for the aqueous solution. However, the interaction of X-G2 with sugars would be much weaker than the hydrophobic interaction with the resin and may not influence the adsorption of X-G2.

Absorption mechanism of DM to the XAD7HP resin

The M_w value of the X-G2 aggregates increased in the presence of certain additives under acidic conditions (Table 3); however, the removal of DM from molasses by adsorbent-column chromatography requires only water as a solvent and the acidification of the molasses. In the present study, we have investigated the pH dependence of X-G2 in aqueous solution, since only sugars should be considered additives in molasses. The LS experiments showed that the A_2 value should be negative and the density should be less than 2.5×10^{-5} g/cm^3 to allow X-G2 to adsorb to the XAD7HP resin (Tables 2 and 3). For example, the adsorption rate for X-G2 was only 21 % at pH 7.3 without salt, because the A_2 value was near zero and the density was greater than 2.5×10^{-5} g/cm^3 (Table 2). The adsorption rate of X-G2 increased to 46 % in 0.1 M NaCl at pH 7.4, because the A_2 value was negative (Table 3). The adsorption rate increased further to 73 % in 1.0 M NaCl at the same pH. Thus, the presence of salt at neutral pH removed the negative charges on the surface of the X-G2 aggregates, and the hydrophobic interactions were restored.

We proposed a model for X-G2 adsorption to the XAD7HP resin (Fig. 3) and used it predict whether the adsorption rate at pH 4.1 would be 72 %, which is similar to that at pH 2.1 (79 %), even though some of the X-G2 carboxyl groups would be negatively charged at pH 4.1. The model is based on the hypothesis that the ionizable groups of the X-G2 aggregates are uniformly distributed on both the inside and outside of the spongy X-G2 structure. At pH 2, there were only a few

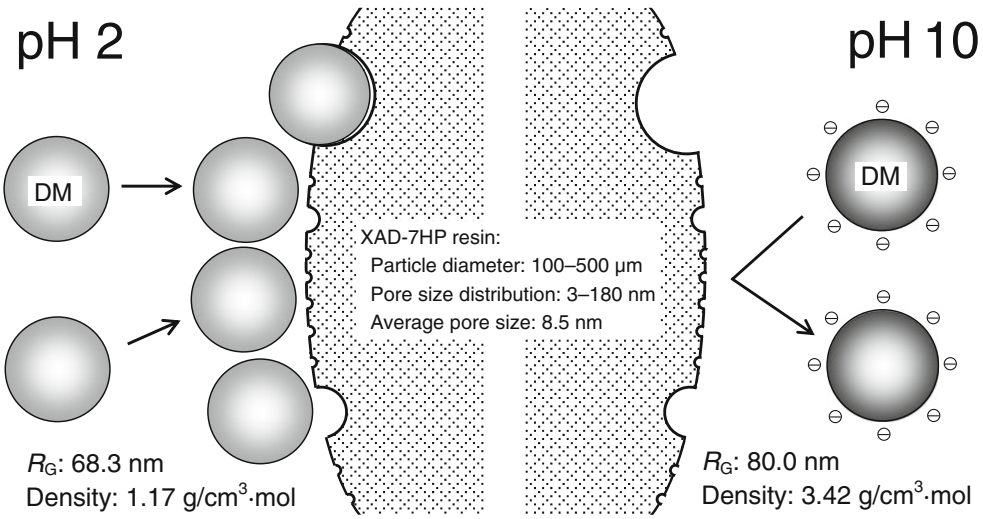

Fig. 4 Adsorption mechanism of the X-G2 particles to the XAD7HP resin

ionized carboxyl groups inside the particle, and an equal number of ionized amino groups. In a previous study, we have demonstrated that the carbon and nitrogen content of the X sample was 43 % and 2 %, respectively (Hatano et al. 2008). Therefore, there should be no ionized groups on the surface of the X-G2 aggregates (Fig. 3). We assumed that the pK_a values of the X-G2 carboxyl groups were similar to those of general organic acids, such as acetic acid, propionic acid, butanoic acid, and valeric acid (pK_a=4–5). About half of the carboxyl groups were estimated to be negatively charged at pH 4; however, most of the ionized groups would be inside the spongy structure of the particle (Fig. 3). Accordingly, most of the surface of the X-G2 aggregates is probably hydrophobic and could adsorb to the XAD7HP resin. However, the values of the M_w and density at pH 6 increased by approximately 4-fold and 3.6-fold, respectively, compared with the corresponding values at pH 2 (Table 2). Therefore, the number of the ionizable groups should also increase in proportion to the molecular density, since the R_G value was constant (Table 2). Furthermore, the estimated pK_a values of 4–5 suggest that almost all the carboxyl groups at pH 6 would be ionized; therefore, the number of negative charges on the X-G2 surface should increase by approximately 4.9-fold (= 4.17/1.71 density × 2) compared with that at pH 4. The hydrophobic region would decrease as the negatively charged surface area increases, and then the adsorption rate would rapidly decrease from 72 % to 43 % (Fig. 3 and Table 2).

The adsorption/desorption mechanism of X-G2 to the XAD7HP resin is summarized in Fig. 4. The resin pore size distribution is 3–180 nm, and the average pore size is 8.5 nm according to the manufacturer. The LS experiments revealed that the R_G value was 66–88 nm for all the pH values. Therefore, our conditions may not fit the general mechanism of adsorption where adsorbates fit into the pores of an adsorbent resin. The main adsorption force would not be governed by electrostatic interactions but by hydrophobic interactions between X-G2 and the resin. At higher pH values, DM desorb from the resin because negative charges appear on the surface of the particle. On the other hand, about half of the carboxyl groups appear to have negative charges at pH 4, but most of the ionized groups are inside the particle due to the spongy structure (Fig. 3). Accordingly, most of the X-G2 surface at pH 4 and pH 2 should be hydrophobic and could adsorb to the resin.

Conclusions

We have demonstrated the physical properties of the functional groups of DM derivatives, the molecular size and shape, and the adsorption/desorption mechanism to the XAD7HP resin. DM derivatives possess a large number of carboxyl groups and the heterogeneous aggregates were formed by intermolecular hydrogen-bonding. The pI values of DM derivatives were estimated to be 1.8–2.0, which indicates that they all are negatively charged over almost the entire pH range. The E_4/E_6 ratios revealed that the physical properties of the X-G1 and X-G2 samples are similar to those of X_{pre} and X_{sup} samples, respectively. Furthermore, the X-G2 particles formed a uniform spherical structure which was low density and spongy, unlike protein molecules (Fig. 3). The spongy structure, the distribution of the negative charges and the aggregability of X-G2 are thought to contribute to the adsorption/desorption actions to the resin. The strength of the adsorption of X-G2 to the resin is probably governed by hydrophobic interactions. Most of the negative charges would appear inside the particle at lower pH values, and the resulting hydrophobic surface could adsorb to the resin (Figs. 3 and 4). At higher pH values, X-G2 is thought to desorb from the resin, because many negative charges appear on the surface of the aggregates. These results are valuable for developing a novel adsorbent for DM and also help to provide a foundation for integrating the physical properties of materials into environmental strategies.

Acknowledgments The authors are grateful to Mr. Satoshi Kikuchi and Kazuhide Suzuki (Gunma University) for their help in the LS and CEC experiments, respectively. Financial support for this research was provided by Fuji Nihon Seito Corporation, by Japan Science and Technology Agency (JST), and partly by the "Element Innovation" Project under the Ministry of Education, Culture, Sports, Science and Technology in Japan.

References

Agarwal CS, Pandey GS (1994) Soil pollution by spent wash discharge: depletion of manganese (II) and impairment of its oxidation. J Environ Biol 15:49–53

Burchard W, Schmidt M, Stockmayer WH (1980) Information on polydispersity and branching from combined quasi-elastic and intergrated scattering. Macromolecules 13:1265–1272

Bustamante MA, Paredes C, Marhuenda-Egea FC, Pérez-Espinosa A, Bernal MP, Moral R (2008) Co-composting of distillery wastes with animal manures: carbon and nitrogen transformations in the evaluation of compost stability. Chemosphere 72:551–557

Chandra R, Pandey PK (2001) Decolourisation of anaerobically treated distillery effluent by activated charcoal adsorption method. Industrial J Environ Prot 2:132–134

Chandra R, Singh H (1999) Chemical decolourisation of anaerobically treated distillery effluent. Ind J Environ Prot 19:833–837

Chuang TC, Lai CL (1978) Study on treatment and utilization of molasses alcohol slop. In: Proceedings of the international conference on water pollution control in developing countries. Asia Institute of Technology, pp 513–524

Coca M, García MT, González G, Peña M, García JA (2004) Study of coloured components formed in sugar beet processing. Food Chem 86:421–433

FitzGibbon FJ, Nigam P, Singh D, Marchant R (1995) Biological treatment of distillery waste for pollution-remediation. J Basic Microbiol 35:293–301

Harris DC (2007) Quantitative chemical analysis, 7th edn. WH Freeman and Company, New York

Hatano K, Kikuchi S, Miyakawa T, Tanokura M, Kubota K (2008) Separation and characterization of the colored material from sugarcane molasses. Chemosphere 71:1730–1737

Hatano K, Kikuchi S, Nakamura Y, Sakamoto H, Takigami M, Kojima Y (2009) Novel strategy using an adsorbent-column chromatography for effective ethanol production from sugarcane or sugar beet molasses. Bioresource Technol 100:4697–4703

Kannabiran B, Pragasam A (1993) Effect of distillery effluent on seed germination, seedling growth and pigment content of *Vigna mungo* (L.) Hepper (C.V.T.9). Geobios 20:108–112

Kim SB, Hayase F, Kato H (1985) Decolourisation and degradation products of melanoidins on ozonolysis. Agric Biol Chem 49:785–792

Kononova VA, Aksenva VB (1963) Hygienic basis for sanitary-protective zones separating living areas and livestock farms. Gig Sanit 28:7–11

Mersad A, Fargues C, Lewandowski R, Decloux M (2003) Sugar colorants: molar masses and retention by cross-flow filtration assessed by size exclusion chromatography on Superose 12. Zuckerindustrie 128:434–442

Pike ER, Pomeroy WRM, Vaughan JM (1975) Measurement of Rayleigh ratio for several pure liquids using a laser and monitored photon-counting. J Chem Phys 62:3188–3192

Provencher SW (1982) CONTIN—a general-purpose constrained regulation program for inverting noisy linear algebraic and integral-equations. Comput Phys Commun 27:229–242

Tanokura M, Tasumi M, Miyazawa T (1976) ^{1}H nuclear magnetic resonance studies of histidine-containing di- and tripeptides. Estimation of the effects of charged groups on the pK_a value of the imidazole ring. Biopolymers 15:293–301